Pergamon

0042-6989(95)00329-0

Vision Res., Vol. 36, No. 17, pp. 2641–2655, 1996

Printed in Great Britain
0042-6989/96 $15.00 + 0.00

Image Formation by the Crystalline Lens and Eye of the Rainbow Trout

W. S. JAGGER*

Received 24 March 1995; in revised form 19 July 1995; in final form 27 November 1995

The image of a distant unresolved point (point image or PI) and modulation transfer function (MTF) of the eye and lens of the trout were recorded with high spatial (0.3 μm) and dynamic (4096 grey levels) resolution for various entrance aperture sizes and focal positions in monochromatic light, and in broadband light simulating sunlight absorbed by a retinal cone pigment. The PI is irregular, with streaks, wisps and speckle, as a result of lens structural irregularity and diffraction of light scattered within the lens and cornea. Maximum diameter of a diffraction-limited aperture area of the eye is about 0.3 mm. Axially spaced multiple foci are caused by irregular and discontinuous zonal spherical aberration. Lens substance dispersion causes strong longitudinal chromatic aberration, resulting in a broadband PI with concentric coloured haloes. Incident linearly polarized light is slightly depolarized in the PI. The nature of the image is discussed relative to lens and cornea structure, optical modelling and vision. Human subjective entoptic phenomena analogous to those observed objectively in the trout are described. Copyright © 1996 Elsevier Science Ltd.

Fish Optics Point spread Resolution Polarization

INTRODUCTION

The relative simplicity of the phylogenetically early teleost eye makes it a useful starting point in understanding vertebrate eye optical function. The cornea is immersed, reducing its power to a negligible level, and the lens supplies nearly all the eye's power. Nearly spherical lens symmetry should permit uniform performance over a wide field. Full spherical symmetry reduces the number of anatomical parameters of a fish lens, and its theoretical optical behaviour can be modelled *a priori* (Jagger, 1992). Insight gained from this modelling applies also to nearly spherical real lenses (Jagger & Sands, 1966). However, such an ideal basic model does not include the semi-random structural irregularity, scattering and diffraction of a real vertebrate eye, and direct observation of an eye's image is needed to understand its actual optical function.

In the star test (Twyman, 1957; Welford, 1978), the image of a distant point object (the point image or PI, described by its point spread function or PSF) in and out of focus is compared to that of a perfect system. Characteristic optical behaviour can be linked to structural features of the imperfect system under test. A perfect optical system, with no geometrical-optical aberrations or structural irregularities to deflect or scatter light, is limited by diffraction to produce an image of finite size, the Airy disk (Born & Wolf, 1980). The larger the entrance aperture of the optics, the smaller this disk will be. A narrower PSF yields a larger MTF, with greater potential image information content. The image formed of a more physiologically relevant extended object can in principle be synthesized from the images of all points on the object.

The information retinal photoreceptors detect depends on the matching of image detail to receptor spacing. If the image structure is too fine, image undersampling causing aliasing and corruption may occur, while if it is too coarse, oversampling will occur, wasting visual system processing capacity. A small degree of undersampling is probably most suitable (Snyder *et al.*, 1986). The fact that retinal photoreceptors can be observed through an eye's optics implies some undersampling (Jagger, 1985; Land & Snyder, 1985).

Few direct measurements have been made on the optical image formed within an eye. Robson & Enroth-Cugell (1978) used a fibre-optic probe to measure the linespread function (LSF) of the cat's image, while Jagger (1988) used a similar method in the eye of the cane toad. The LSF was recorded by sweeping the image of a distant fine bright line object across the fibre-optic collecting aperture at the retina. Image fine structure detected is limited by the collecting aperture size. Also, the LSF will show less fine structure than the PSF because it integrates the PSF along the line. The LSF measured was not perfectly smooth, suggesting that the PSF was still less smooth. Scattered light was also detected far from the image.

*Department of Ecology and Evolutionary Biology, Monash University, Clayton, Victoria 3168, Australia.

The image formed on the retina can be observed through the eye's optics. (Westheimer & Campbell, 1962; Wässle, 1971; Krueger & Moser, 1971; Jagger, 1988). These results are affected by the absorbing, scattering and reflecting properties of the retina and other structures, as well as by a second passage through the optics, all of which degrade the LSF or PSF and mask fine structure.

The image of a distant unresolved point is examined directly in the star test by focusing a microscope on the image formed by the lens or eye. Using the star test visually, Sroczyński (1979) described the image of a point formed by a trout lens as poor compared to that of manufactured optics, consisting of a "more or less deformed main image surrounded by many secondary images, which originate from the longitudinal as well as lateral variation in zonal foci". He also noted the poor contrast of the image of a lamp.

The star test with high spatial and dynamic resolution is used here to examine the detailed structure of the trout lens and eye point image at and near focus. This is then related to the known optical structure of the lens and eye (Jagger & Sands, 1996). Corneal and lens cells are comparable in size to the wavelength of visible light, and interact with it to degrade optical behaviour. The MTF, a comprehensive measure of imaging ability, is determined directly using a grating resolution test. Monochromatic light, although somewhat unnatural, is used to gain insight into the lens and eye imaging process, while more natural broadband light is used to simulate daylight image formation in the eye. Visual consequences of the nature of the image formed by the fish eye and lens are discussed. Clear parallels occur between subjectively observed human entoptic phenomena and objective observations in the trout eye.

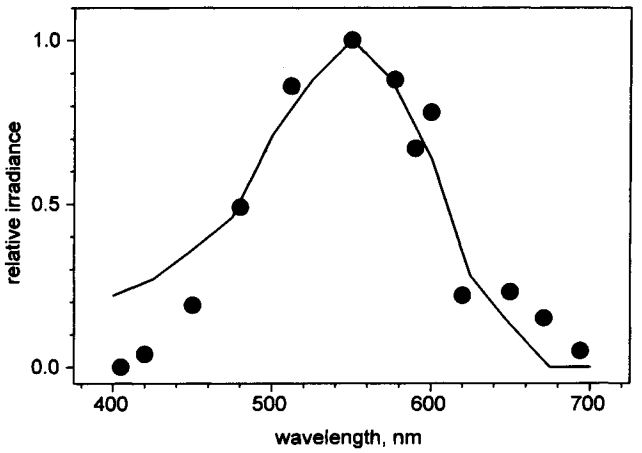

FIGURE 1. Measured CCD response to the broadband light used to simulate sunlight absorbed by a cone pigment (solid circles). The line is the sea level solar spectrum combined with a 550 nm peak cone pigment absorption spectrum.

METHODS

Definitions, conventions and abbreviations

Definitions and conventions are those of modern optical engineering and optics (Moore, 1966; Born & Wolf, 1980). Abbreviations are: CCD, charge-coupled device; FL, focal length; FWHM, full width at half-maximum; LCA, longitudinal chromatic aberration; LSA, longitudinal spherical aberration; LSF, linespread function; MTF, modulation transfer function; NA, numerical aperture; PI, point image of a distant unresolved point; PSF, point spread function describing the PI; SD, standard deviation; SF, spatial frequency.

The fish eye and lens preparation

Eyes were obtained from rainbow trout (*Oncorhychus mykiss*) as described by Jagger & Sands (1996). For the eye preparation, the posterior sclera and retina were removed, with cornea and vitreous intact. The eye was placed facing downward through a hole in a plastic disk, lined with petroleum jelly to effect a pressure seal outside the corneal limbus, into a chamber containing distilled water. The chamber floor was of high quality flat optical glass. Negative pressure of 300 mm water column was applied to this chamber to simulate the pressure difference across the cornea due to intraocular pressure in life, and the posterior part of the preparation was immersed in buffered trout Ringer. For the lens preparation, the cornea and iris were also removed without disturbing the lens. The stiff cartilaginous sclera maintained its shape and held the lens and vitreous in their normal position. This preparation was suspended in Ringer facing downward. The star test could be performed first on an eye, and then on its lens. Solutions were maintained at about 15 °C. Lens and cornea remained clear during measurements, made within 1 hr after death.

Apparatus and procedures

The star test point source (Jagger & Sands, 1996) was produced by focusing light from a halogen lamp into a tapered glass light guide of tip diameter 0.2 mm. Monochromatic light was produced by placing an interference filter of centre wavelength 550 nm and FWHM 7 nm before the focusing optics. To simulate the chromatically aberrated image of a white sunlit point object detected by hypothetical cones of 550 nm peak absorption, spectral composition was used having CCD camera response approximating the combination (by multiplication at each wavelength) of the solar spectrum at sea level (Zissis & Larocca, 1978) with the absorption spectrum of this cone pigment (Partridge & DeGrip, 1991). Trout cone absorbance peaks at 576, 531 and 434 nm (Hawryshyn & Hárosi, 1994) surround this hypothetical 550 nm cone pigment, and chromatic PSF broadening and the MTF measured for 550 nm should be similar to those detected by the actual pigments. Solar spectral composition would apply for a fish near the surface at clear midday; time of day, atmospheric and water conditions and depth would alter this spectrum (Nicol, 1989). Wideband interference filters in parallel were placed before the focusing optics so that the

spectrum detected by the CCD camera approximated the solar-cone pigment curve (Fig. 1). These spectral points were measured using calibrated interference filters of FWHM 10 nm. This curve is zero at wavelengths shorter than 400 nm because of source and detector limitations. This will result in some underestimation of the true chromatic PSF broadening because the low pigment *cis* band extends the combined pigment-solar spectrum to about 350 nm.

Light from the 2 m distant point source was reflected up the microscope axis by a high-quality front-surface flat mirror and entered the eye preparation in the physiological direction. An objective (Zeiss Jena Apo 40×, NA 0.95) of NA sufficiently high to accept all rays from the fish lens exit aperture (of NA 0.38) was immersed in the fluid and focused on the image formed by the fish lens or eye. This objective was tested under immersion to have less than 1 μm LCA for 450 to 700 nm. An inverted objective of FL similar to that of the trout lens (Carl Zeiss Plan 25×, NA 0.45), when substituted for it formed an Airy disk at focus and circular diffraction rings out of focus as expected for high-quality optics. None of the image fine structure seen with the trout optics was observed when the microscope objective was substituted. The geometrical-optical image diameter of the 0.2 mm point source 2 m distant formed by ideal optics of FL 6 mm (the FL of the trout) is 0.45 μm, while the Airy disk diameter at 550 nm formed of an infinitesimally small source by a lens of entrance aperture diameter 5 mm and FL 6 mm (as in the trout) is 1.2 μm. The point source is therefore unresolved as required for the star test. The PI was photographed or recorded by a cooled (to reduce thermal noise) computer-controlled digital CCD camera of square field with 165 × 192 pixels, 12 bit linear dynamic resolution (pixel values from 0 to 4095, or 4096 grey levels) and variable integration time. Usual magnification gave a frame width of 50 μm, with pixel spacing 0.3 μm, a small fraction of trout axial retinal cone spacing (about 12 μm). Image processing removed CCD dark signal non-uniformities and residual thermal noise. This system allows radiometric measurement and examination of image detail over a dynamic range greater than that possible using photography. Three-dimensional landscape plots of the PSF (diffraction solids) display detailed image structure and dynamic range, while a histogram shows the relative frequency of PI pixel values. Rotationally averaged PSF profiles were plotted by a program that located the peak pixel value in the image and plotted the mean pixel values within concentric annuli about the peak and their SD vs mean annulus radius. A series of PIs located axially inside, at, and outside best focus was recorded at positions set with a stage height micrometer dial indicator. PIs were recorded for various centred circular substage aperture sizes. Polarizing properties of the lens and eye were determined with linear polarizing filters before the preparation and after the objective.

For the grating test, gratings of various SFs on clear film in front of a backlit window subtending 1.3 deg against a dark background were presented to the lens or eye. Grating image modulation

$$M(\text{fish}) = (I\text{max} - I\text{min})/(I\text{max} + I\text{min})$$

at each SF was calculated, where Imax and Imin are the recorded CCD signals at maximum and minimum. Comparison at each SF with measured modulation M(obj) of a high-quality microscope objective of FL and NA similar to those of a trout lens (Carl Zeiss Plan 25×, NA 0.45) in place of the fish optics yielded the fish MTF:

$$\text{MTF(fish)} = M(\text{fish})/M(\text{obj})$$

The small error resulting from use of square rather than sinusoidal gratings was neglected (Jagger & Muntz, 1993). Results presented were typical of at least five eyes or are averages from five eyes (Fig. 11).

RESULTS

Monochromatic lens PI and PSF

A typical monochromatic lens PI (Fig. 2) is irregular, with radial streaks and diffraction structure. Three-fold symmetry as in this PI was seen in more than half of the lenses, while others showed irregular structure [Fig. 7(a)]. The streaks are broken into bright segments and spots. The landscape plot [Fig. 2(b)] shows a steep mountain with sharp peaks and a rapid descent to base level. Spurs extend from the peak onto the base plain, corresponding to streaks seen in the PI. The rotationally averaged PSF [Fig. 2(c)] shows a sharp central peak, then a slower fall-off with distance from the peak, dropping to about 0.2 of the peak value at 5 μm. The PSF radius at half-maximum is about 1.5 μm. The SD of pixel values at a given radial distance results from irregularity of the image structure.

Monochromatic eye PI and PSF

The PI of the same eye before corneal removal is shown in Fig. 3. The irregularity and streaks obvious in the lens PI are covered by a more uniform speckle pattern. Many radially extending rays are also present. The landscape plot shows the PSF mountain with multiple small peaks, with a broader base of the PSF mountain than for the lens alone. The rotationally averaged PSF again shows a sharp central peak, but away from the peak it does not decay as rapidly as does the lens PSF. The PSF radius at half-maximum is about 3 μm, and at 5 μm radius its value is about 0.3 of the peak value.

Broadband eye PI and PSF

The PI of the trout eye in broadband light simulating daylight (Fig. 4) is somewhat broader than that in monochromatic light. Speckle structure is still evident, but with less contrast. Observed in colour, the PI shows concentric colour bands. The landscape plot [Fig. 4(b)] shows a smoother and broader PSF mountain with less prominent secondary peaks. The rotationally averaged PSF plot [Fig. 4(c)] shows a broad PSF, and a less

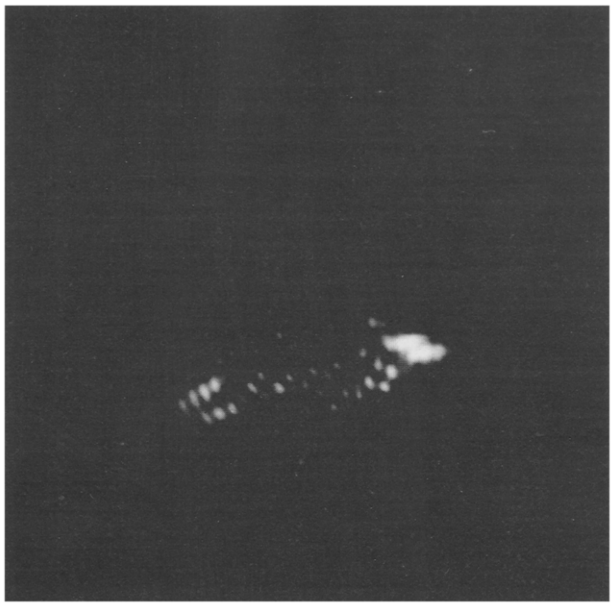

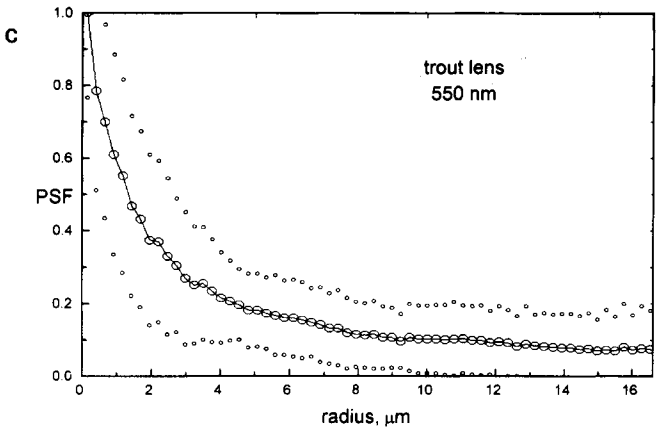

FIGURE 2. (a) PI of a trout lens in monochromatic light (550 nm, FWHM 7 nm). Frame size: 50×50 μm. (b) Landscape plot of the PSF over the frame. (c) Rotationally averaged PSF (connected large circles), peak normalized to 1; small circles are $\pm$SD.

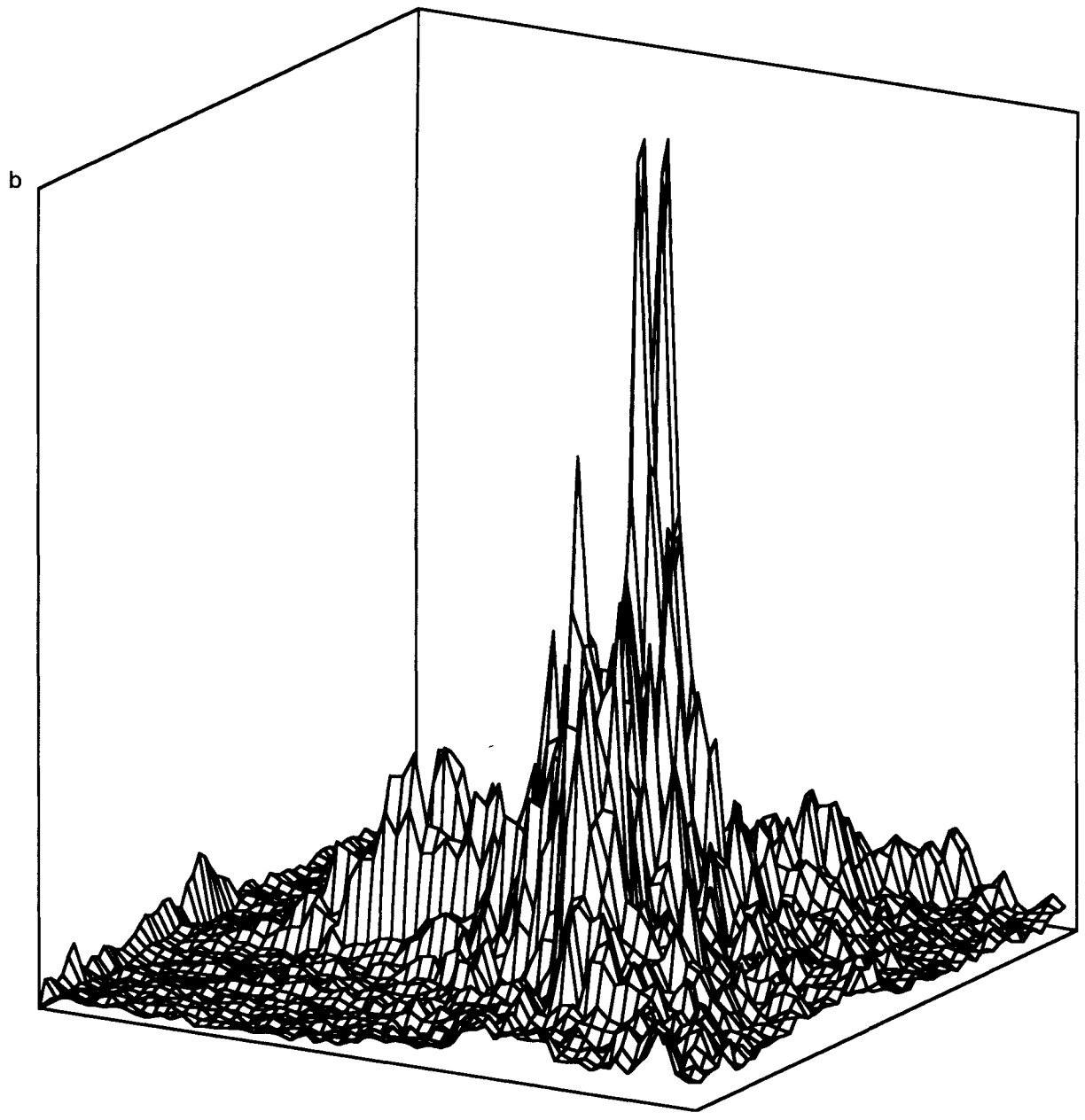

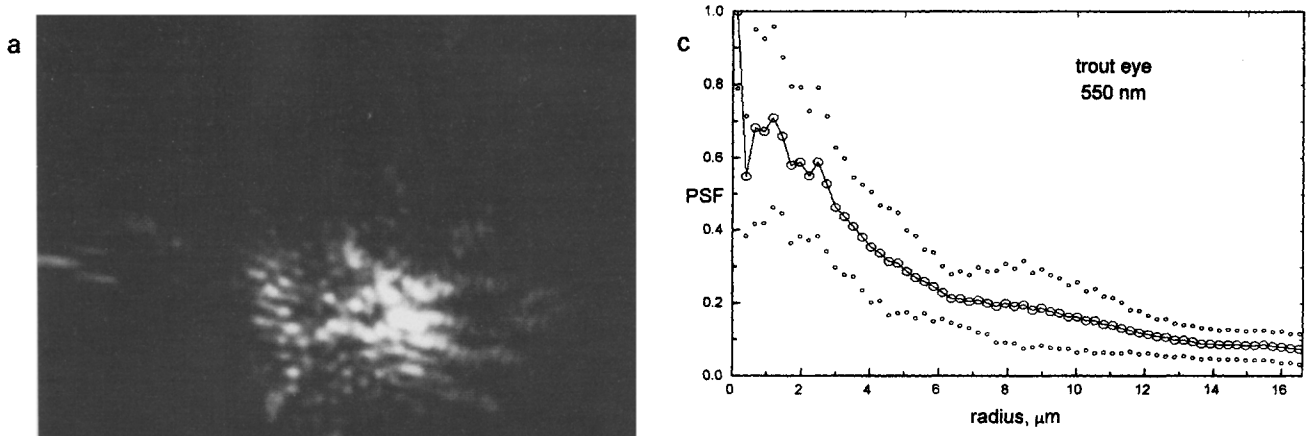

FIGURE 3. (a) PI of a trout eye in monochromatic light (550 nm, FWHM 7 nm). Frame size: 50×50 μm. (b) Landscape plot of the PSF over the frame. (c) Rotationally averaged PSF (connected large circles), peak normalized to 1; small circles are $\pm$SD.

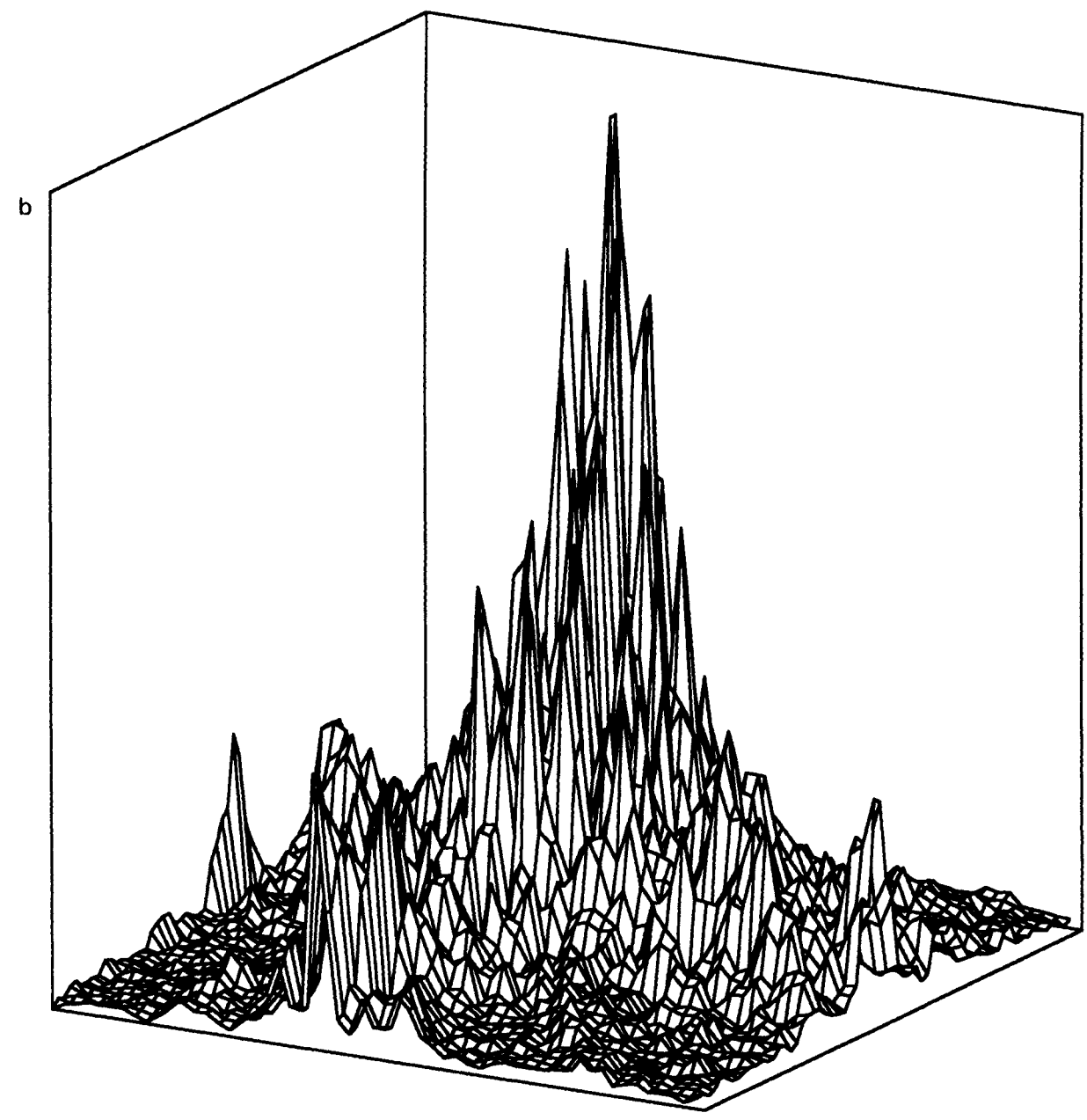

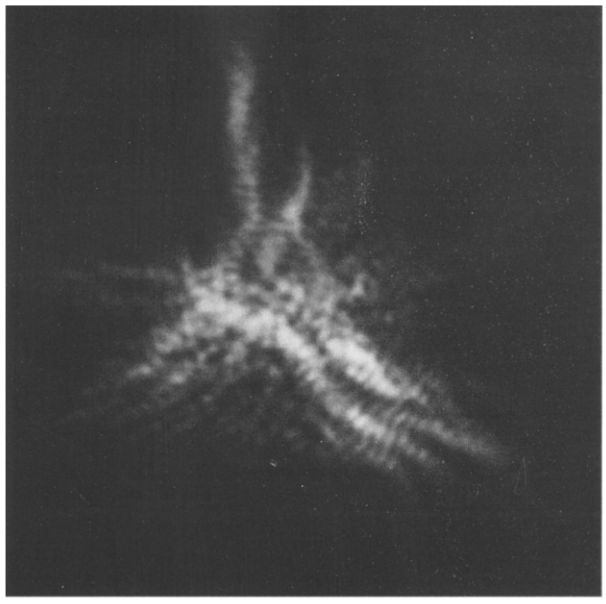

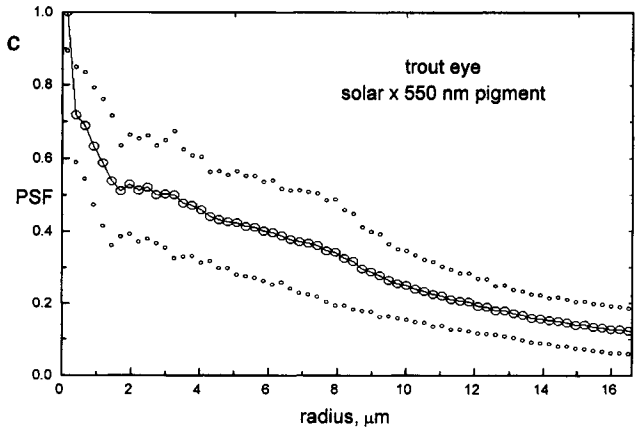

FIGURE 4. (a) PI of a trout eye in broadband light simulating sunlight absorbed by a cone pigment. Frame size: 50 × 50 μm. (b) Landscape plot of the PSF over the frame. (c) Rotationally averaged PSF (connected large circles), peak normalized to 1; small circles are $\pm$SD.

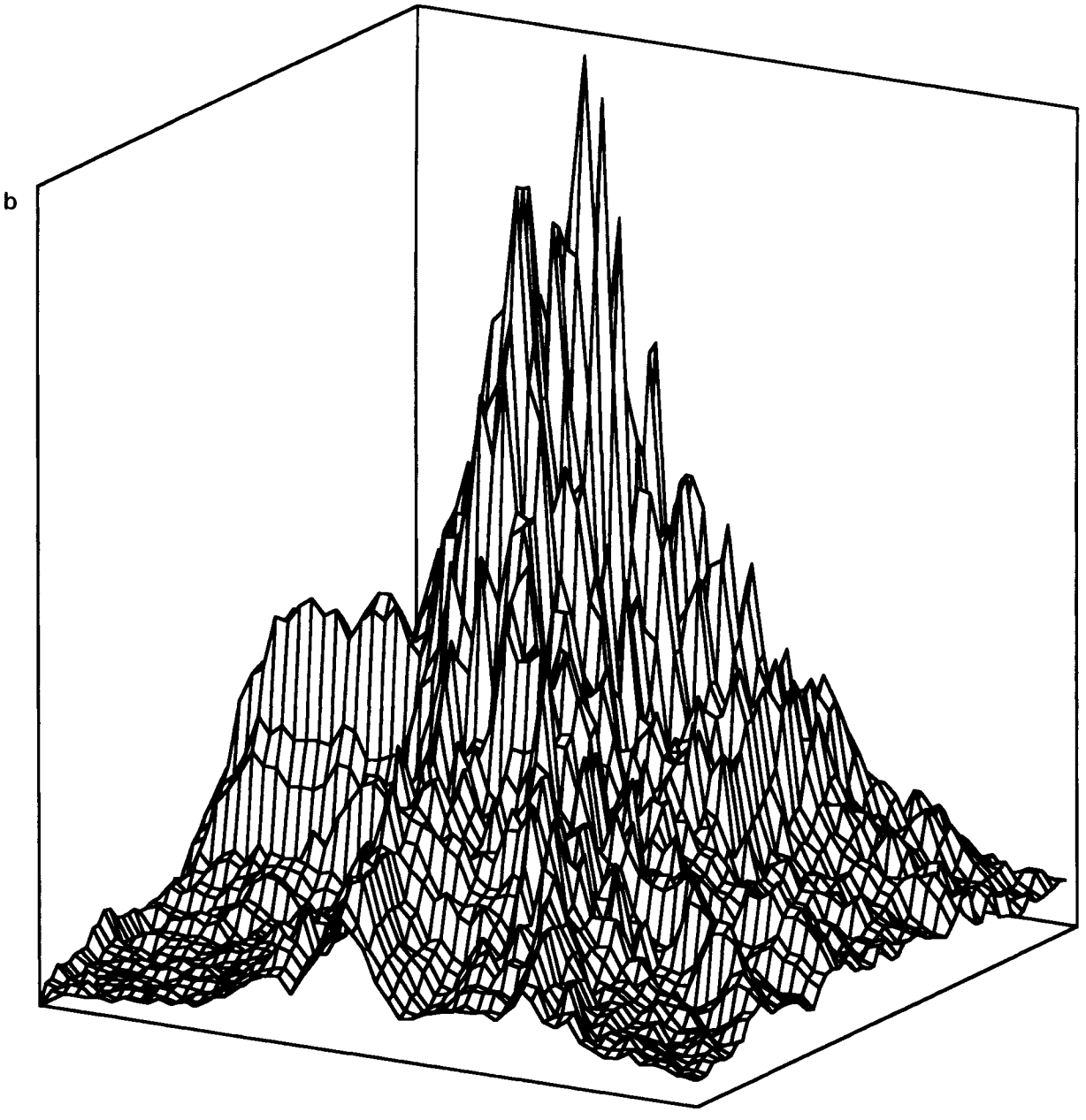

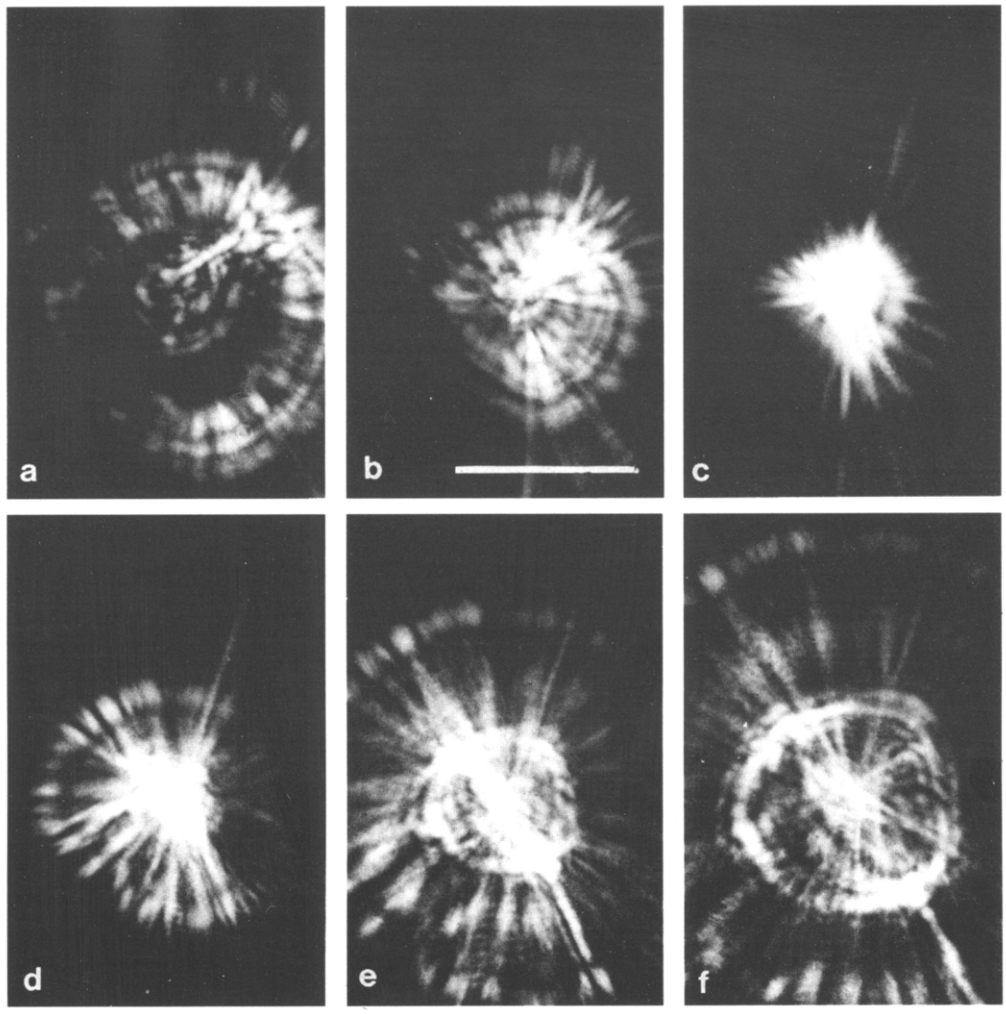

FIGURE 5. Sequence of photographs through focus of the trout lens PI. Frame sequence is spaced 150 μm axially, from inside to outside focus. Scale is 100 μm. Exposure was chosen to make faint features distant from the centre visible; the centre of the PI is overexposed in frames near focus.

prominent central peak. From Fig. 4(c), the PSF radius at half-maximum is about 2.5 μm, with a height at 5 μm radius of about 0.40 of the peak value.

Monochromatic PI focus series for the trout lens and faint detail surrounding the image centre

Figure 5 shows a sequence of PI photographs through focus for a trout lens at full aperture. The exposure used shows fine detail in the outer image, while the focused image centre is overexposed. Starting from 300 μm within (nearer the lens) focus [Fig. 5(a)], caustic patterns gradually condense to focus and expand again as focus is passed. Ring caustic structure is visible away from focus, with concentric bright and dark rings which are not perfectly circular. Radial streaks appear during the sequence, as well as segmenting (caused by diffraction) of streaks. Occlusion of half of the entrance aperture blocks out half the image, including the streaks; this would not occur if the streaks themselves were due to diffraction. The image is irregular, and the position of best focus is not precisely defined.

Figure 6 is a plot of the diameter of two superimposed ring caustics vs focus position of a typical trout lens. Caustic diameter was measured with micrometre calipers on PI photographs. One ring pattern focuses at a different axial location from the other, and the slope or speed of convergence to focus differs for the two.

Monochromatic PI aperture series for the lens and eye

Figure 7(a) shows a PI series for circular substage aperture sizes full (5 mm), 2 mm and 1 mm for the trout lens in monochromatic light. As the aperture becomes smaller, the radial streaks disappear, and the image displays fewer but larger speckles. Figure 7(b) shows a similar series for the trout eye. As the aperture decreases from full size, the rotationally averaged PSF (Fig. 8) falls at intermediate radii, but its central peak (the highest speckle) becomes broader. A single speckle should have the form of an Airy disk (shown superimposed), which will become broader at smaller apertures. For full aperture, the Airy disk lies below the CCD resolution, but for smaller apertures, the Airy disk matches the shape of the sharp central peak speckle. This correspondence is clearly shown in Fig. 9. The points are a radiometric scan

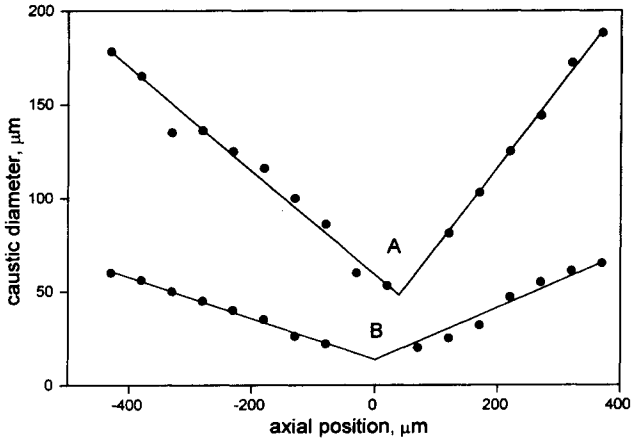

FIGURE 6. Diameter of distinct separate faint ring caustics present in a lens PI vs axial position. Rays from outer zones of the lens converge more rapidly as focus position is changed. Caustic A originates from the outer zones of the lens, while caustic B originates from inner zones. The position of best focus for caustic A lies farther from the lens than that of caustic B.

across the 12 bit CCD image of a single isolated speckle from Fig. 7(b) formed by an eye with substage entrance aperture 1.0 mm and FL 6.0 mm. The solid curve shown, fit to the points, is a Gaussian, which Snyder (1979) showed is a close approximation to the Airy profile. Its measured width at half-maximum is 2.86 μm, in good agreement with the expected Airy profile width of 2.5 μm (Moore, 1966; Snyder, 1979; Born & Wolf, 1980).

The statistical frequency of pixel values in the monochromatic PI of a focused eye is shown by the histogram of Fig. 10. It is similar in form to that of a lens alone.

Depolarization by the lens and eye

The intensity principal transmittance ratio for linear polarization (measured intensity for parallel polarizers divided by that for crossed polarizers; Shurcliff, 1962) measured in the image of a point object using an objective of FL and NA similar to those of the trout lens (Carl Zeiss Plan 25×, NA 0.45) in place of the trout eye was greater than 500. Replacing the objective with a trout lens or eye reduced this to between 10 and 20 over the visible spectrum. Linearly polarized light incident on the trout optics therefore becomes slightly depolarized with a degree of polarization between 90 and 95%. The lens or eye does not act as a linear polarizer; transmitted light does not vary upon rotation of a single polarizer.

Monochromatic and broadband lens and eye MTF

Figure 11 shows the average MTF for the trout lens and eye in monochromatic light as well as broadband light simulating the absorption spectrum of a retinal pigment combined with the solar spectrum. In the lens, the full aperture broadband and monochromatic MTF drop rapidly to low values by 5 or 10 c/deg. However, for smaller apertures, the MTF falls less rapidly, especially in monochromatic light. For a 1 mm aperture, the

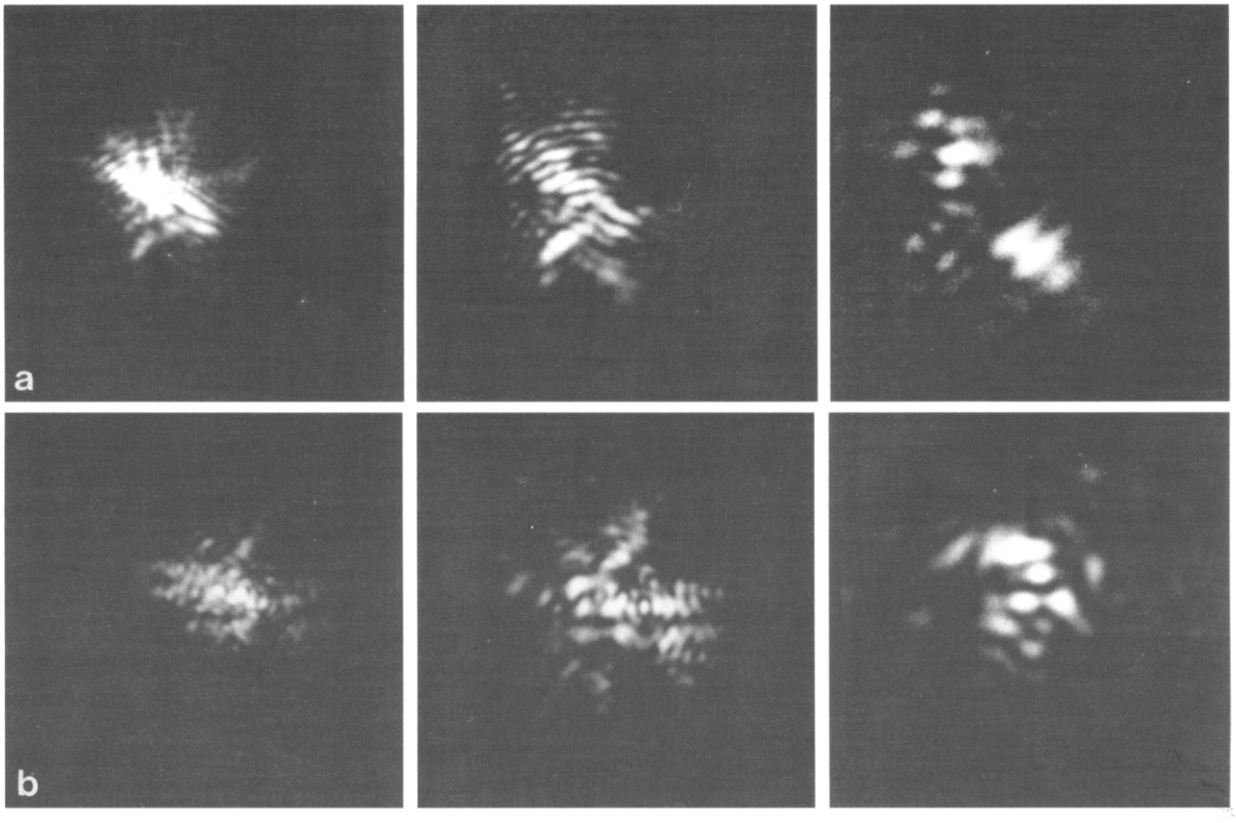

FIGURE 7. (a) PI of a trout lens at best focus (top row) for apertures of 5 (left), 2 (centre), and 1 mm diameter (right). (b) Similar sequence for a trout eye (bottom row). Scale: 20 μm.

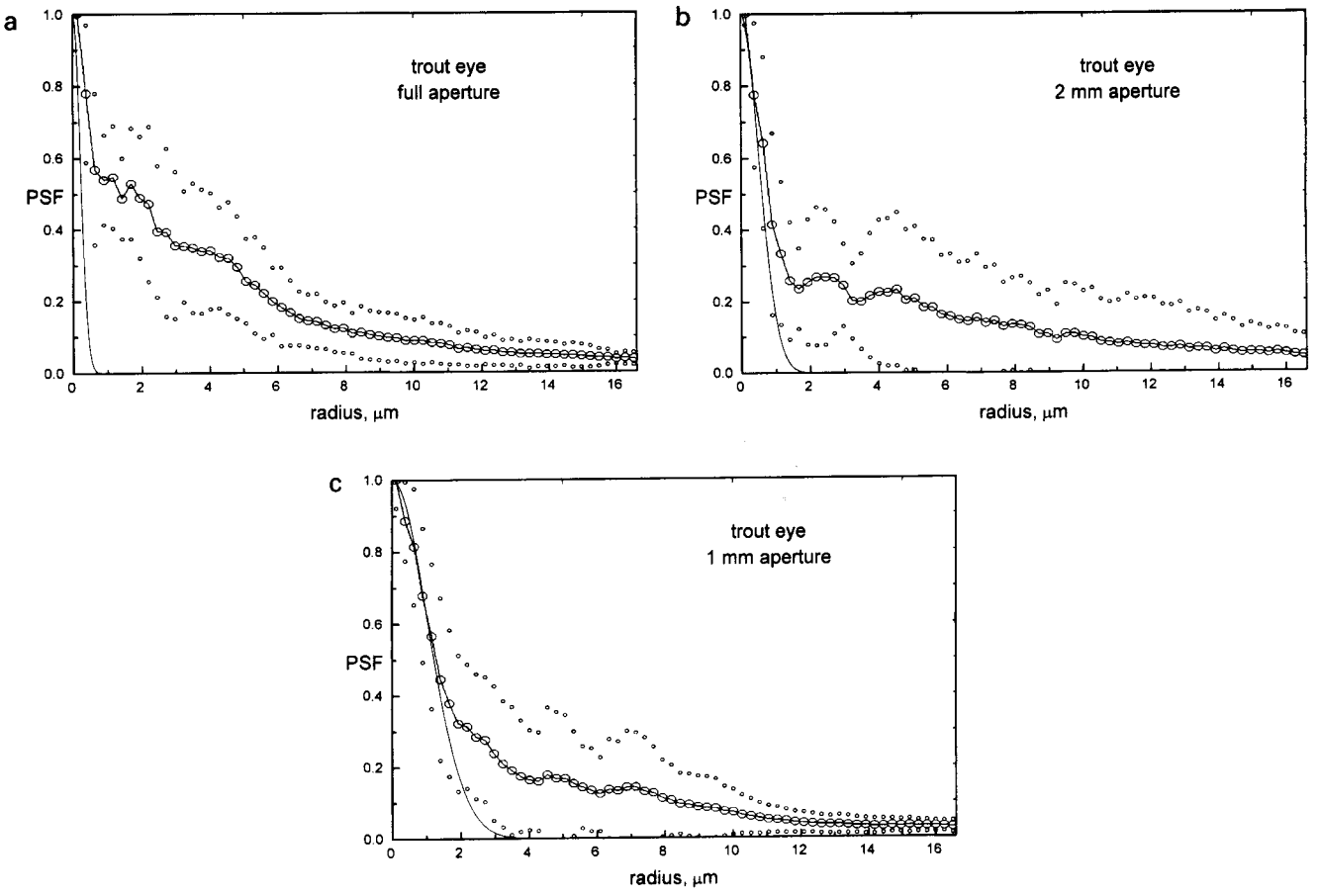

FIGURE 8. Rotationally averaged PSF (connected large circles) for the images of Fig. 7(b); small circles are ±SD. The Airy disk profile (smooth curve) is also shown for each aperture size.

monochromatic lens MTF is still 0.15 or 0.2 out to 25 c/deg.

In the trout eye, the full aperture MTF for both monochromatic and broadband light again falls rapidly and reaches a low level by 5 or 10 c/deg. As in the lens, for monochromatic light the MTF remains higher for smaller apertures. However, for the most natural case, the eye in broadband light, MTF curves differ little for different sized apertures.

Multiple axially spaced foci are seen in the image of gratings of SF greater than 2 c/deg by the trout optics. Changing microscope focus brings successive grating images into focus, which also show lateral phase dislocations. The general contrast is low, with local variations, probably a result of superimposed unfocused images.

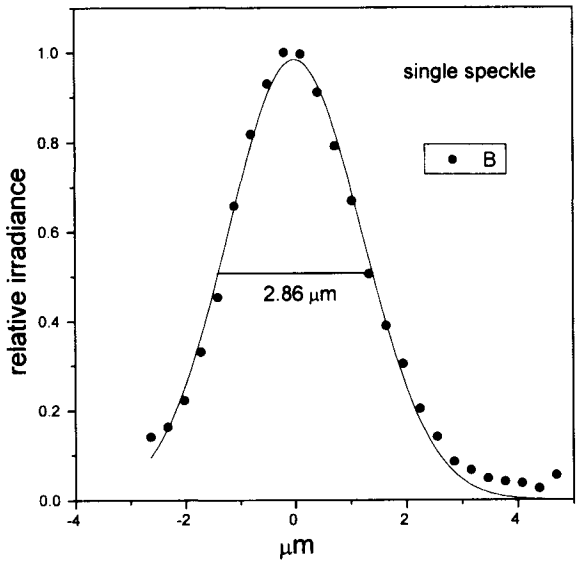

FIGURE 9. The profile of an isolated single speckle. Points are relative irradiance along a line across a single speckle of the PI formed by an eye with a 1 mm diameter substage aperture. The points fit a Gaussian (solid line), which is a good theoretical approximation to an Airy disk profile. The FWHM is 2.86 μm.

DISCUSSION

Differences between the trout PSF and that of ideal optics

The PSF of ideal optics, e.g., of a high quality microscope objective, is a rotationally symmetric Airy disk, with diameter inversely proportional to the entrance aperture diameter. For an entrance pupil diameter of 5 mm and FL of 6 mm (as for the trout), the Airy disk diameter to the first dark ring is 1.2 μm and its FWHM is 0.5 μm. Faint concentric diffraction rings surround the focused disk. A unique well-defined focus exists, independent of wavelength. Depolarization of linearly polarized light is very small.

The PI of trout optics is larger than the Airy disk (and is

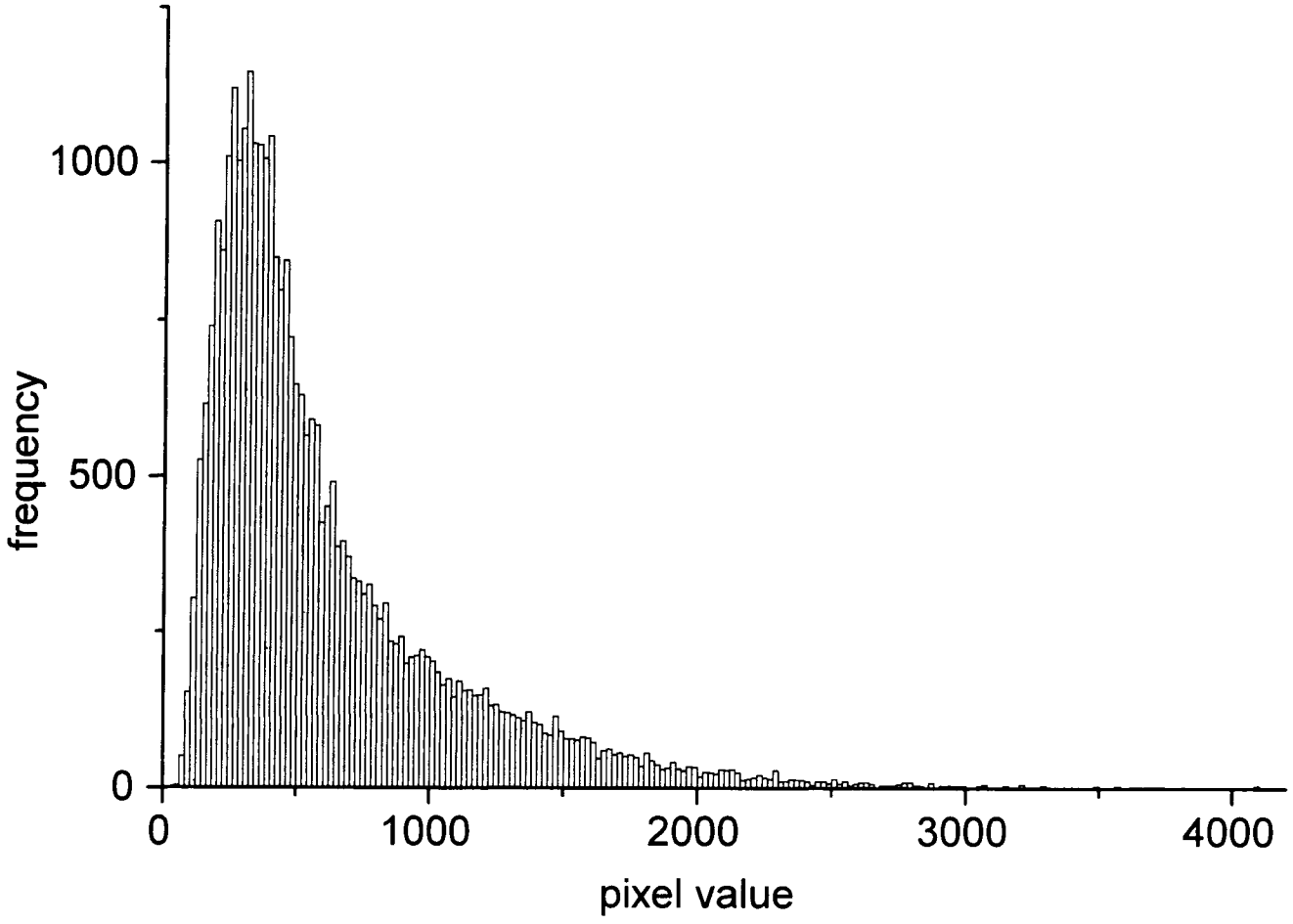

FIGURE 10. Histogram showing the frequency of PI pixel irradiance values for an eye in monochromatic light.

hence not diffraction limited), and it is not rotationally symmetric, containing fine structure, including radial streaks, irregular diffraction patterns, and speckle. Its rotationally averaged PSF decays approximately exponentially from the shoulders of a sharp central peak, and differs greatly in form from an Airy disk. The axial position of best focus is ill-defined, and frequently more than one focus is discernible. Strong LCA widens the broadband PI into a multicoloured disk, and linearly polarized light is somewhat depolarized.

PI features and their structural origins

Streaks and lack of rotational symmetry in the PI. The lens PI has little rotational symmetry; streaks, asymmetries and irregular diffraction patterns dominate its structure [Figs 2, 5 and 7(a)]. An axially symmetric model provides a basis for the trout optics by concentrating light in a small focal area, rotationally symmetric on axis, but additional mechanisms are needed to account for observed PI fine structure. The frequently observed 3-fold rotational symmetry, with associated diffraction patterns, seen in the trout lens PI (Fig. 2) resembles catastrophe caustic patterns reported by Berry & Nye (1977) and Berry *et al.* (1979), caused by refractive structure 3-fold rotational symmetry. The source of this PI 3-fold axial symmetry is also probably a lens structural 3-fold axial symmetry, perhaps distributed within the lens, similar in refractive effect to the triangular water droplet used by Berry *et al.* (1979). It is probably not a lens suture, as fish lenses generally have only line sutures (Yatabe, 1933; Yamasaki, 1953; Koch, 1951).

A further deviation from perfect axial rotational symmetry is the faint radial streaks and wisps of the PI (Figs 2 and 5), which appear as spurs on the landscape plot, and cover a wide area around the image centre. They originate in the outer lens zones, and disappear upon stopping down the lens. They originate from the radially oriented refractive structure in the lens outer zones seen in Schlieren photographs [Fig. 12(a)]. The linkage between the two is apparent from photographs of planes between the lens and the focused image. At the lens plane, the Schlieren photograph shows these radial patterns clearly [Fig. 12(a)]. At an intermediate plane, [Fig. 12(b)], these radial patterns start to merge into image streaks. Near focus (Fig. 5), streaks connect ring caustics and extend beyond. At best focus [Fig. 5(c)], faint streaks extend from the concentrated image, giving the PI a multipointed starlike appearance. The structural origin of these radial patterns is probably fluctuations in lens fibre density and spacing.

Diffraction, speckle and scattering. A more random diffraction pattern, or speckle, occurs in the eye PI, largely due to the cornea. An Airy disk is surrounded by unbroken concentric diffraction rings, but in the more

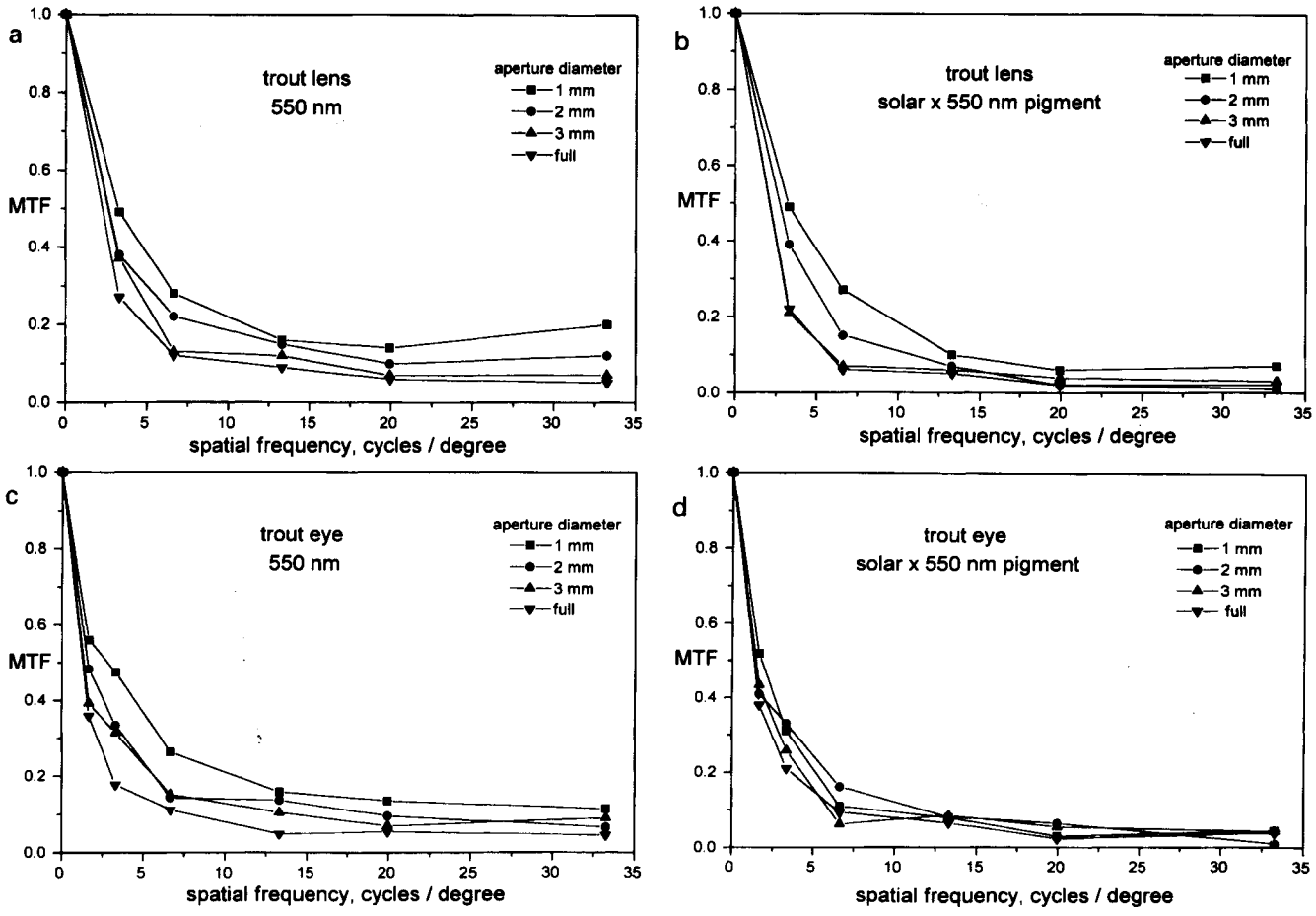

FIGURE 11. (a) Measured trout lens MTF in monochromatic light (550 nm, FWHM 7 nm) and (b) broadband light simulating sunlight absorbed by a 550 nm cone pigment. (c) Measured trout eye MTF in monochromatic light and (d) broadband light. Curves are averages from five lenses or eyes.

complex lens PI, the diffraction pattern breaks up and also becomes more complex. Scattering by the cornea superimposes additional random complexity upon the diffraction pattern, resulting in the observed eye PI speckle. The speckle pattern indicates randomness of scatter but reveals little about the scatterers themselves (Dainty, 1975; Goodman, 1975; Hariharan, 1987); the trout eye speckle pattern is very similar to that resulting from turbulent atmospheric scatter in the image of an unresolved star formed by the 5 m aperture Palomar telescope (Dainty, 1975). The light used here of bandwidth 7 nm is sufficiently coherent to allow the speckle to be readily observed. Less coherent broad-spectral bandwidth light reduces speckle contrast, as speckle points at different wavelengths do not coincide.

Each speckle point is an Airy disk of size dictated by the full system aperture size, irrespective of the system's correction. A speckle point is the diffraction-limited image of the object, and the eye PI is a two-dimensional array of diffraction-limited images (Fig. 7). The irradiance profile of a single speckle is that of an Airy disk of form and width close to that expected from diffraction theory (Fig. 9). The size of the "seeing unit" or maximum diffraction limited aperture diameter d is related to the full aperture diameter D and the number of speckles n by (Labeyrie, 1976):

$$d = D/\sqrt{n}$$

The value of d, about 0.3 mm, was calculated from the approximate number of strong speckle points in the PI of the eye of Fig. 7. This size aperture would produce a single diffraction-limited image (one speckle).

The intensity probability distribution function in a uniform speckle pattern is exponential, yielding a small number of intense single speckles well above the underlying undiffracted PI, analogous to "monster" ocean waves. Intense single speckles are apparent in the landscape plots and in the rotationally averaged PSF plots for monochromatic light. The irradiance histogram (Fig. 10) has a peak at low pixel values due to the background, while its shape at higher pixel values results from combination of the undiffracted PI and the exponential speckle statistics. The expected few intense speckles cause a small tail at high pixel values.

Scattering also deflects light away from the PI peak, broadening the PI at low values. The high sharp speckle peak, seen especially in a monochromatic PI, raises the question of whether this diffraction-limited peak could improve visual resolution. Because the width of this peak for full aperture is about an order of magnitude smaller

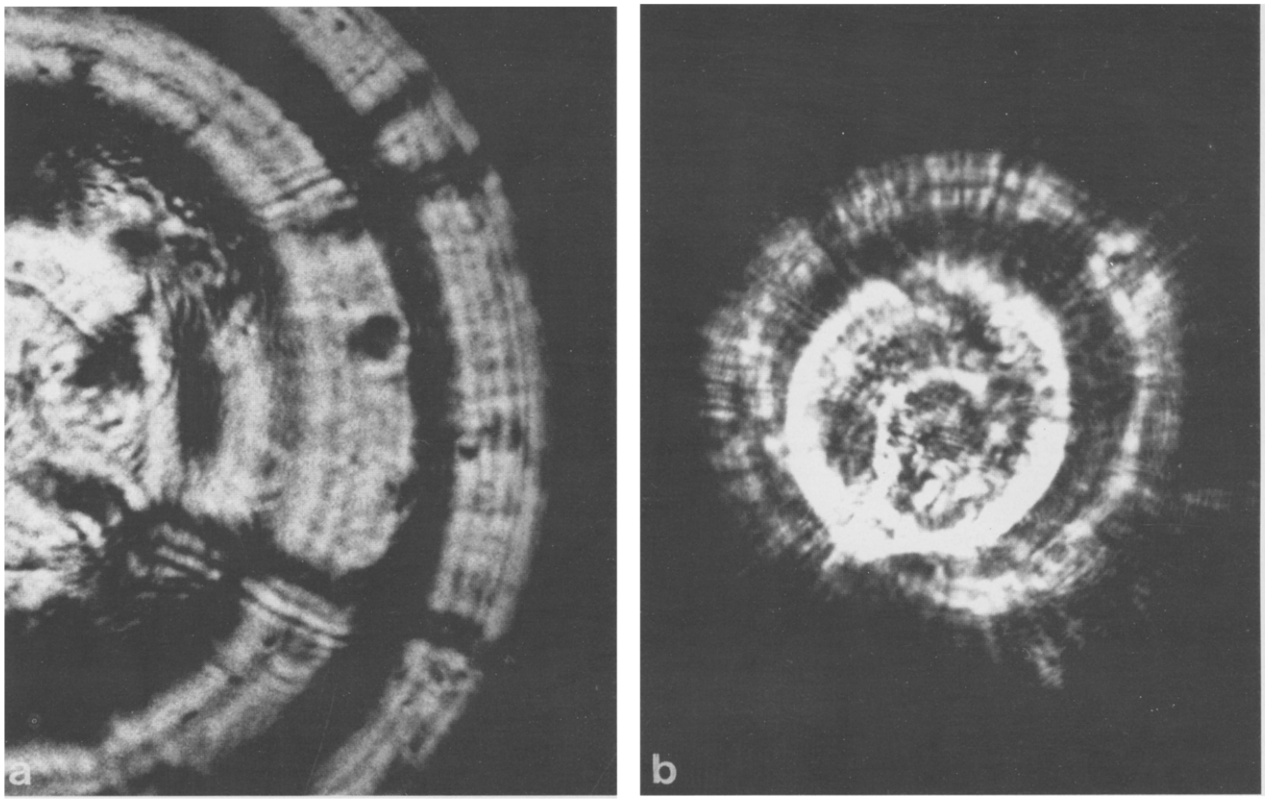

FIGURE 12. (a) Detail from a Schlieren photograph at the plane of the lens exit aperture. In the outer zones, concentric layers and radial streaks and condensations are evident, reflecting lens structure (see Jagger & Sands, 1996). (b) Irradiance pattern at a plane intermediate between a lens and the focused image. The lens structure has partially merged into image structure. Compare with images at and near focus (Fig. 5).

than receptor spacing, and little of the total PI power is contained in the peak, it is unlikely that the potential high resolution (about 150 c/deg) of such a peak is useful for ordinary vision. These peaks probably cause the significant MTF values measured at high SF in monochromatic light. They could be useful in hyperacuity tasks and high-resolution ophthalmoscopy.

Multiple foci. Sroczynski (1979) observed secondary images separated laterally and axially. Present results indicate that lateral multiple images are largely due to diffraction (speckle), while axially separate multiple images are caused by lack of smoothness in the lens index gradient, resulting in multiple zonal foci. Jagger & Sands (1996) demonstrated annular lens zones of different focus using a Schlieren test. The result is distinct ring-shaped caustics (Fig. 5) that focus at different locations than other parts of the lens (Fig. 6). These caustics are nearly concentric but not perfectly circular, and appear as bright rings separated by dark spaces. The caustic that condenses to a focus rapidly as axial position is changed is clearly due to a lens zone of greater radius than that which condenses more slowly. Some fish have multiple receptor layers at different depths in the retina (Locket, 1977), and multiple foci could simultaneously focus an object at different retinal depths or increase accommodative range, with decreased contrast.

Longitudinal chromatic aberration (LCA). Jagger & Sands (1996) showed by measuring chromatic axial focus shift that the trout lens has large uncorrected LCA caused by dispersion of lens material of about 4% of the FL (7 dioptres for a 5 mm lens) in the range 450–700 nm. In broadband light the PI is a superposition of monochromatic PI patterns, only one of which can be in focus on a given image surface. The broadband light used here applies to only one cone system; an image of a sunlit object detected simultaneously by the three cone systems can be optimally focused for only one if they are coplanar. Superposition of images that are out of focus to varying degrees will decrease contrast of fine structure apparent in a monochromatic PI and widen the broadband PI (Fig. 4). Lateral chromatic aberration is negligible because of spherical symmetry.

Depolarization of linearly polarized light. Hawryshyn & Bolger (1990) reported that trout can detect linearly polarized light. Present results indicate that information about the linearly polarized light environment is readily transmitted by the eye's optics. Light scattering probably causes the small depolarization present.

Grating resolution and visual function

In principle the trout eye and lens MTF can be calculated by Fourier transforming the LSF derived from the PSF. However, image fine structure would cause MTF elevation at high SF that is irrelevant to vision. The MTF was therefore measured directly from the image contrast of gratings of various SFs. Comparison of these

MTF curves (Fig. 11) allows assessment of the separate effects of the cornea, LCA, and pupil size upon the MTF. These curves are of similar form, dropping rapidly with increasing SF to low values by about 5 or 10 c/deg.

The cornea has relatively little effect on the MTF. In the eye and lens, LCA degrades the MTF somewhat, especially for smaller apertures and higher SF. This occurs because broadening due to LCA is a larger fraction of grating bar width at high SF.

Decreasing aperture size has little effect on the eye MTF in broadband light, but increases the lens and eye MTF in monochromatic light. The trout iris is immobile in life, perhaps because it would offer little improvement in resolution of natural scenes. Stopping down the lens or eye in monochromatic light would be expected to increase the MTF by reducing streak structure, scattering and multiple foci. The relatively high MTF (above 0.15) for the lens in monochromatic light at SFs up to 25 c/deg apparently results from high central speckle peaks. Figure 8(c) shows that for a 1 mm aperture, the eye PSF central peak is diffraction-limited, with form similar to an Airy disk, implying an MTF extending to about 30 c/deg as in Fig. 11(c).

Full-aperture eye MTF curves drop to low values by 5–10 c/deg. Axial double cone spacing in brown trout of similar size is about 12 μm (Lyall, 1957), which corresponds to a 6 mm FL to an anatomical resolution of 4.3 c/deg, perhaps increasing to about 6 c/deg on the visual axis. Image quality is therefore approximately matched to the sampling mosaic. A non-zero MTF at higher SF is of no direct use and may lead to aliasing. However, an MTF curve of adequate magnitude at the anatomical resolution SF may trail off at higher SFs with little visual consequence (Snyder *et al.*, 1986). The relatively low resolution of trout optics is not an adaptation to the inability of natural waters to transmit high spatial frequencies; Jagger & Muntz (1993) showed high and low SFs are transmitted nearly equally well by clear natural waters although turbid waters will attenuate all strongly.

Optical modelling of the eye

A basic axially symmetric model of the trout lens and eye is given by Jagger & Sands (1996) which predicts average FL, LSA, LCA and image quality. Evidence was given for secondary structural features expected to affect image formation. Their quantitative incorporation into a complete model is in principle possible by treating each feature as a small perturbation on the basic structure and calculating results using physical-optical formalism, including diffraction. In practice this is difficult because of the complex semi-random nature of the secondary structure. The more direct course of action taken here is to identify the effects of each feature in the observed images. However, the basic model PSF and MTF may be compared to those measured, keeping secondary structure and diffraction in mind. The exact form of the model PSF and MTF is very sensitive to model parameters. However, the basic model PSF should be no broader than that observed, and the model MTF should be no lower than that observed.

Monochromatic lens PSF and MTF. The axial monochromatic PSF of the model lens [Fig. 13(a), Jagger & Sands, 1996] reaches a half-peak value at a radius of about 1 μm and zero at about 4 μm. A typical measured PSF [Fig. 2(c)] reaches half-maximum at about 1 μm radius, and decays slowly (approximately exponentially) with increasing radius. It also shows a large variation around its mean curve. The measured curve is centred on the most intense speckle [Fig. 2(b)], which may range well above the broader mean PSF. The slow decay results from broadening effects of secondary structure, which also cause random deviation from the mean curve. However, the comparison is in general as expected: the sharp PSF of the basic model is broadened and degraded in a random fashion by secondary structure of the real lens.

The monochromatic model lens MTF on axis [Fig. 13(c), Jagger & Sands, 1996] can be compared with the measured MTF of Fig. 11 for full aperture. The model lens MTF lies well above the measured MTF below 25 c/deg.

Monochromatic eye PSF and MTF. A similar comparison holds for the model eye PSF [Fig. 13(b), Jagger & Sands, 1996] and a typical measured eye PSF (Fig. 3). The model PSF falls to 0.5 of the peak value at a radius of less than 2 μm. Beyond that, it is close to zero. This slight broadening of the eye model PSF compared to the lens model PSF is caused by the cornea; the model was optimized for the lens alone. The measured eye PSF again shows a sharp peak, centred on the highest speckle [Fig. 3(c)]. The remaining curve then decays slowly. Again, the central speckle [Fig. 3(b)] causes the sharp central peak, well above the mean PSF. The model eye axial MTF lies well above the measured MTF curve.

Analogies with the human eye

Several human subjective entoptical phenomena are analogous to objective observations on the optics of the trout eye. Their highly singular nature indicates similar structural origins. By inference, these features may also be expected in other vertebrates. Young (1801), Helmholtz (1909) and Palmer (1991) discuss the irregular multipointed star form of the human PI and its origin in optical irregularity. The focused trout PI also appears as a multipointed irregular star [Fig. 5(c)]. Diagrams of the unfocused human PI presented by these authors show similarities to the trout PI (Figs 2 and 5). The trout eye PI with an unfocused ring caustic surrounding a central focused caustic with intermediate radial rays resembles strongly the drawings by Young of unfocused PIs in his own eye (Fig. 13). Helmholtz discusses how the irregular structural features of human optics gradually transform into the irregular features of its PI. This transformation can be seen in the trout lens in the sequence from a Schlieren photograph at the lens exit pupil plane [Fig. 12(a)], to an intermediate plane [Fig. 12(b)], to an out-of-focus PI [Fig. 5(b)], and finally to a focused PI [Fig. 5(c)].

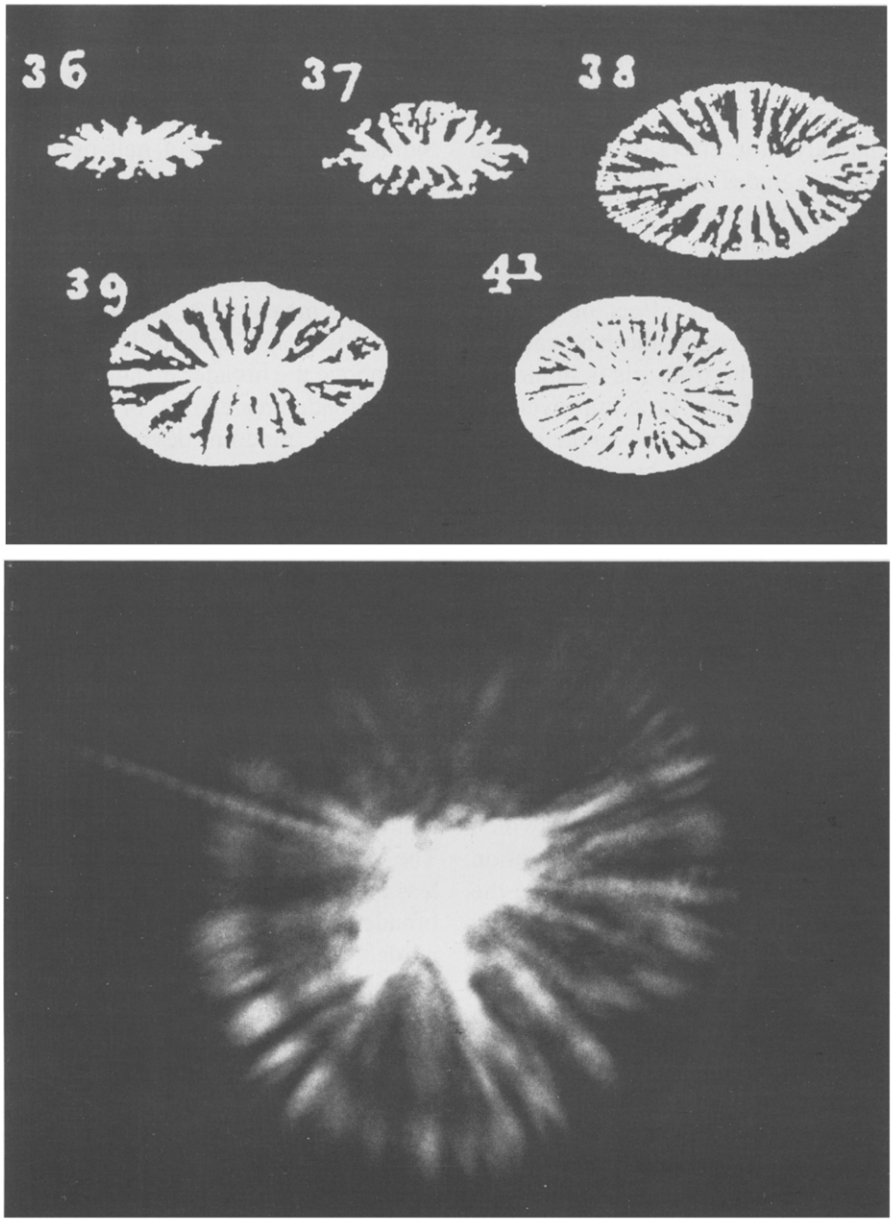

FIGURE 13. Numbered drawings by Young (1801) of the subjective unfocused images formed by his own eye of a distant point object, compared to an unfocused trout eye PI.

Objective measurements of the human LSF (Westheimer & Campbell, 1962) show that it decays from its peak in a similar manner to the trout PSF.

Helmholtz discusses the separate superimposed ciliary corona, due to scatter within the eye causing speckle analogous to that in the trout eye. The distinctness of the ciliary corona from PI irregularity is demonstrated by moving an occluding card across the pupil; the irregular features of the PI are directly occluded by the card, but the corona is not, as expected from its origin. Simpson (1953) describes innumerable rapidly moving points of light that are clearly speckle (the term was not in use at the time) in the ciliary corona in monochromatic light. In white light, fine radial rays due to secondary diffraction effects appear which give the ciliary corona its name. Helmholtz also describes discontinuities of human eye LSA, analogous to those seen in the Schlieren photographs of the trout lens.

REFERENCES

Berry, M. V. & Nye, J. F. (1977). Fine structure in caustic junctions. *Nature, 267*, 34–36.

Berry, M. V., Nye, J. F. & Wright, F. J. (1979). The elliptic umbilic catastrophe. *Philosophical Transactions of the Royal Society of London A, 291*, 453–484.

Born, M. & Wolf, E. (1980). *Principles of optics*. Oxford: Pergamon.

Dainty, J. C. (1975). Stellar speckle interferometry. In Dainty, J. C. (Ed.), *Laser speckle and related phenomena*, (pp. 9–75). Berlin: Springer.

Goodman, J. W. (1975). Statistical properties of laser speckle patterns Dainty, J. C. *Laser speckle and related phenomena*, xxx–xxx. Springer, Berlin.

Hariharan, P. (1987). *Optical holography.* Cambridge: Cambridge University Press.

Hawryshyn, C. W. & Bolger, A. E. (1990). Spatial orientation of trout to partially polarized light. *Journal of Comparative Physiology A, 167*, 691–697.

Hawryshyn, C. W. & Harosi, F. I. (1994). Spectral characteristics of

visual pigments in rainbow trout (*Oncorhychus mykiss*). *Vision Research, 34*, 1385–1392.

Helmholtz, H. von (1909). *Handbuch der physiologischen Optik*. Hamburg: Voss. English translation: (1962). Southall, J. P. C. (Ed.), *Helmholtz's treatise on physiological optics*. New York: Dover.

Jagger, W. S. (1985). Visibility of photoreceptors in the intact living cane toad eye. *Vision Research, 25*, 729–731.

Jagger, W. S. (1988). Optical quality of the eye of the cane toad *Bufo marinus*. *Vision Research, 28*, 105–114.

Jagger, W. S. (1992). The optics of the spherical fish lens. *Vision Research, 32*, 1271–1284.

Jagger, W. S. & Muntz, W. R. A. (1993). Aquatic vision and the modulation transfer properties of unlighted and diffusely lighted natural waters. *Vision Research, 33*, 1755–1763.

Jagger, W. S. & Sands, P. J. (1996). A wide-angle gradient-index optical model of the crystalline lens and eye of the rainbow trout. *Vision Research, 36*, 2623–2639.

Koch, C. (1951). Sulla fine struttura della lente cristallina dei Pesci (Scomberoidi). *Atti Della Società Oftalmologica Italiana, XII*, 108–114.

Krueger, H. & Moser, E. A. (1971). Refraktion und Abbildungsgüte des Froschauges. *Pflügers Archiv der gesamte Physiologie, 326*, 334–340.

Labeyrie, A. (1976). High-resolution techniques in optical astronomy. *Progress in Optics, XIV*, 47–87.

Land, M. F. & Snyder, A. W. (1985). Cone mosaic observed directly through the natural pupil of a live vertebrate. *Vision Research, 25*, 1519–1525.

Locket, N. A. (1977). Adaptations to the deep sea environment. In Crescitelli, F. (Ed.), *Handbook of sensory physiology VII/5*, (pp. 67–192). Berlin: Springer.

Lyall, A. H. (1957). The growth of the trout retina. *Quarterly Journal of Microscopical Science, 98*, 101–110.

Moore, W. J. (1966). *Modern optical engineering*. New York: McGraw-Hill.

Navarro, R. (1985). Incorporation of intraocular scattering in schematic eye models. *Journal of the Optical Society of America A, 2*, 1891–1894.

Nicol, J. A. C. (1989). *The eyes of fishes*. Oxford: Clarendon.

Palmer, D. A. (1991). Entoptic phenomena. In Cronly-Dillon, J. R. (Ed.), *Vision and visual dysfunction 1*, (pp. 345–356). London: Macmillan.

Partridge, J. C. & DeGrip, W. J. (1991). A new template for rhodopsin (vitamin A_1 based) visual pigments. *Vision Research, 31*, 619–630.

Robson, J. G. & Enroth-Cugell, C. (1978). Light distribution in the cat's retinal image. *Vision Research, 18*, 159–173.

Shurcliff, W. A. (1962). *Polarized light*. Cambridge, Massachusetts: Harvard University Press.

Simpson, G. C. (1953). Ocular haloes and coronas. *British Journal of Ophthalmology, 37*, 450–486.

Sivak, J. G. & Bobier, W. R. (1978). Chromatic aberration of the fish eye and its effect on refractive state. *Vision Research, 18*, 453–455.

Snyder, A. W. (1979). Comparative physiology and evolution of vision in invertebrates In Autrum, H. (Ed.), *Handbook of sensory physiology*, VII/6A, (pp. 225–313). Berlin: Springer.

Snyder, A. W., Bossomaier, T. R. J. & Hughes, A. (1986). Optical image quality and the cone mosaic. *Science, 231*, 499–501.

Sroczyński, S. (1976). Die chromatische Aberration der Augenlinse der Regenbogenforelle (*Salmo gairdneri* Rich.). *Zoologisches Jahrbuch Physiologie, 80*, 432–450.

Sroczyński, S. (1979). Über ein einfaches Verfahren zur Messung der Brennweite der Fischkristallinsen. *Zoologischer Anzeiger, 203*, 1–11.

Twyman, F. (1957). *Prism and lens making*. London: Hilger & Watts.

Wässle, H. (1971). Optical quality of the cat eye. *Vision Research, 11*, 995–1006.

Welford, W. T. (1978). *Star tests*. In Malacara, D. (Ed.), *Optical shop testing* (pp. 351–379). New York: John Wiley & Sons.

Westheimer, G. & Campbell, F. W. (1962). Light distribution in the image formed by the living human eye. *Journal of the Optical Society of America, 52*, 1040–1045.

Yamasaki, Y. (1953). Beiträge zur vergleichenden Anatomie des Sehorgans. 3. Über den Linsenstern bei den Knochenfischen. *Yokohama Medical Bulletin, 4*, 325–332.

Yatabe, T. (1933). Beitrag zur Kenntnis der Morphologie der Linsennähte, nebst Bemerkungen über ihre Entwicklung und Regeneration. *Keijo Journal of Medicine, 4*, 93–246.

Young, T. (1801). On the mechanism of the eye. *Philosophical Transactions of the Royal Society B, 92*, 23–88.

Zissis, G. J. & Larocca, A. J. (1978). Optical radiators and sources. In Driscoll, W. G. (Ed.), *Handbook of optics* (pp. 3-1–3-83). New York: McGraw-Hill.

Acknowledgements—Australian Research Council grant A09330801 supported this work. The author thanks P. J. Sands, W. R. A. Muntz and A. Hughes for helpful discussions.